Indonesian Journal of Science & Technology

Journal homepage: http://ejournal.upi.edu/index.php/ijost/

Structural and Physicochemical Tuning of Binary and Ternary Mn-Based Layered Double Hydroxides via Alkali-Free Synthesis for Advanced Material Applications

Nazrizawati Ahmad Tajuddin[*], *Nur Alia Maisarah Binti Saiful Bhari, Nur Alyaa Binti Kamal, Mohamad Hidayat Haider, Siti Hasnah Kamarudin*

Universiti Teknologi MARA, Selangor, Malaysia

[*]Correspondence: E-mail: nazriza@uitm.edu.my

ABSTRACT

This study explores the alkali-free synthesis of binary (MnCo) and ternary (MnCoCr) layered double hydroxides (LDHs) to enhance structural and physicochemical properties relevant to advanced catalytic systems. The materials were synthesized using an ammonium nitrate buffer, followed by controlled ageing and calcination. Characterization included PXRD, BET, TGA, FESEM, and FTIR techniques. The ternary MnCoCr LDH demonstrated improved crystallinity, larger surface area, and more uniform morphology compared to the binary MnCo LDH. These enhancements occurred because chromium altered interlayer spacing and cation interactions, promoting better nucleation and structural integrity. The findings suggest that careful control of metal composition and synthesis conditions can effectively tailor LDH properties. This approach supports sustainable materials engineering and opens new possibilities in catalysis, adsorption, and energy storage applications.

ARTICLE INFO

Article History:
Submitted/Received 15 Apr 2026
First Revised 20 May 2026
Accepted 15 Jul 2026
First Available Online 16 Jul 2026
Publication Date 01 Apr 2026

Keyword:
Alkali-free,
Layered double hydroxide,
Physiochemical,
Secondary,
Tertiary.

1. INTRODUCTION

Layered double hydroxides (LDHs), commonly known as hydrotalcite-like compounds, are a class of ionic lamellar materials composed of positively charged brucite-like layers separated by charge-balancing anions and interlayer water molecules [1]. Since their discovery in the 19th century, LDHs have been studied for their versatility in catalytic applications, anion exchange, adsorption, and electrochemical energy storage [2]. Their structural flexibility and tunable composition allow researchers to tailor their physicochemical properties to specific applications, making them one of the most promising materials in the field of advanced materials engineering [3, 4].

Traditionally, LDHs are synthesized through alkali co-precipitation, often using sodium hydroxide or potassium hydroxide to maintain alkaline pH conditions [5]. However, the use of strong alkalis poses significant environmental and operational drawbacks. Alkaline residues can lead to reactor corrosion, generate excessive wastewater due to repeated washing steps, and cause leaching of active species, ultimately compromising catalyst performance [6, 7]. These challenges necessitate the development of alternative synthesis methods that are both effective and sustainable. Alkali-free synthesis, which replaces corrosive agents with benign acidic salts like ammonium nitrate, offers a green alternative while preserving material performance [8, 9].

Despite growing interest in alkali-free methods, research on their application in manganese-based LDHs remains limited, particularly for systems incorporating multiple metal cations such as cobalt and chromium. Ternary LDHs with three different metal cations have shown the potential for enhanced functionality due to synergistic effects between the constituent metals [10, 11]. However, the physicochemical behavior of MnCoCr LDHs synthesized via alkali-free routes remains poorly understood, and existing studies often focus on more commonly used Zn- or Ni-based systems [12, 13].

This study addresses that gap by investigating the structural and physicochemical effects of incorporating chromium into MnCo LDH using an alkali-free synthesis approach. The objective is to evaluate how the ternary composition alters crystallinity, interlayer spacing, morphology, and thermal stability compared to binary systems. The novelty of this work lies in three aspects: first, it demonstrates the successful synthesis of MnCo and MnCoCr LDHs entirely without alkali agents, which is rarely reported for Mn-based systems; second, it reveals a unique crystallization behavior driven by Cr inclusion that promotes lattice expansion and uniformity without requiring hydrothermal conditions; and third, it introduces Mn-based ternary LDHs as sustainable candidates for catalysis and energy storage, an area still underexplored in current materials science research. Through this exploration, the study contributes to the broader goal of developing environmentally responsible and application-specific advanced materials.

2. METHODS

Manganese (II) sulfate-1-hydrate was purchased from Bendosen, whilst cobalt (II) nitrate and chromium (III) nitrate were bought from R&M Chemicals. The ammonium nitrate was obtained from R&M Chemicals and was used as a buffer in the preparation of a buffer solution. Manganese (II) sulfate-1-hydrate, [$Mn(SO)_4.H_2O$] (100, 1.5 M), cobalt (II) nitrate hexahydrate, [$Co(NO_3)_2{\cdot}6H_2O$] (100, 1.5 M), and chromium (II) nitrate, [$(Cr(NO)_3)2$] (100, 1.5 M) solution have been diluted using distilled water into 100 mL volumetric flasks each. A volume ratio of 4:1:1 Mn:Co:Cr and 4:1 Mn:Co in 100 mL of mixed metal nitrate solution has been prepared. The solution has been stirred at room temperature with a constant pH of 8.5.

DOI: https://doi.org/10.17509/ijost.v11i1.87940
p- ISSN 2528-1410 e- ISSN 2527-8045

2 M of ammonium nitrate (acidic salt) has been added as a buffer. The mixture then underwent an ageing process at 65°C overnight under stirring. Then, the alkali-free solid product has been filtered and washed with deionized water until the pH reaches 7. The sample was first dried in the oven at 100 °C for 24 hours. This sample was denoted as a fresh sample with the acronym F-MnCoCr. Next, this white solid product has been calcined under a flow of 20 mL/min^{-1} at 425°C for 5 hours based on the TGA result of fresh MnCoCr LDH. This sample was denoted as a calcined sample with the acronym C-MnCoCr. This method has been adapted from Ref (Erma et al., 2020). This method has also been applied in the synthesis of MnCo LDH, except the pH was changed while stirred at constant with a constant reading of 9.0, and the calcined temperature was set at 375°C. The sample was denoted as a fresh sample with the acronym F-MnCo. Next, the white solid product has been calcined under a flow of 20 mL/min at 375°C for 5 hours based on the TGA result of fresh MnCo LDH. This sample was denoted as a calcined sample with the acronym F-MnCo.

The physicochemical properties of samples were characterized using powder X-ray diffraction (PXRD), thermogravimetric analysis (TGA), Brunauer-Emmett-Teller (BET), Field Emission Scanning Electron Microscopy (FESEM), and Fourier transform infrared spectroscopy (FTIR). Powder X-ray Diffraction (PXRD) performed by the PANalytical X'pert PRO model was operated at 40 kV and 40 mA using Cu-kα. Measurements were made with a diffraction angle of 2θ from 8 to 90° at a speed of 1.2°/min. The chemical composition of major elements present in the material, the structure, and the crystallography of the synthesized catalyst samples were identified using PXRD. The samples were further analyzed using a high-performance modular simultaneous TGA and DTA/DSC thermal analyzer (ambient/2400 °C) under a nitrogen flow rate of 30 mL/min in dry air with a temperature range of 0 to 800 °C and a heating rate of 20 mL/min to determine the thermal transition of the sample. SETARAM Evolution 18 (TG-DSC/DTA) was used to evaluate the interlayer water and carbonate content at a heating rate of 800 °C at 10 m/min under nitrogen flows.

The surface area (SA) and pore size distribution measurements were obtained with the Quantachrome Autosorb iQ$_2$ instrument. N_2 gas was used as the adsorbate at 77 K. The surface area was measured using a multipoint approach by Brunauer, Emmett, and Teller (BET), and the pore size distribution was calculated using the Barret, Joyner, and Halenda (BJH) desorption method with a gradually increasing temperature in three steps and a ramp rate of 10. Before analysis, samples were degassed at 120 °C for 12 hours to get rid of any adsorbed species. With a Schottky emitter at an accelerating voltage of 3.0 kV and a beam current of 1.0 mA, a JOEL JSM-7600F apparatus was used to study the surface morphologies of the produced materials. Before examination, the samples were placed on Au-coated silicon chips in ethanol after being ultrasonically dispersed. The apparatus allows for high-resolution imaging and analysis of the samples. FTIR was used to identify the functional group and chemical bonds of the samples by producing an infrared absorption spectrum using a Perkin Elmer (Model: Spectrum One) FTIR spectrometer at a wavenumber of 4000–600 cm^{-1}.

3. RESULTS AND DISCUSSION

MnCo and MnCoCr LDHs have been successfully synthesized and characterized by PXRD, TGA, BET, FESEM, and FTIR. The PXRD patterns for fresh LDH, F-MnCo, and F-MnCoCr are shown in **Figure 1(a)**, whereas the results for calcined LDH, C-MnCo, and C-MnCoCr are shown in **Figure 1(b)**. The discovered crystalline phases for F-MnCo are due to reflections of 2θ at 25°, 33°, 38°, 41°, 46°, 51°, 52°, and 61°, which correspond to the HKL planes of (003), (101), (102), (108), (109), (110), (113), and (116). These planes were identical to those in [14-16].

DOI: https://doi.org/10.17509/ijost.v11i1.87940
p- ISSN 2528-1410 e- ISSN 2527-8045

All of the peaks mentioned above were narrow, with a single crystalline phase and duplets at 51 and 52°, confirming the successful synthesis of the LDH [17]. These diffraction peaks also correspond well with the standard JCPDS card no. 22-0700, thereby confirming the successful formation of the LDH phase. The identical diffraction patterns, but with stronger peaks, have appeared on F-MnCoCr (**Figure 1(a)**). The position of duplets in the PXRD patterns might be shifted, but they are all positioned ranging from 40°- 65° [13, 14, 16]. These results demonstrated that LDH was successfully synthesized.

Figure 1(b) depicts the calcined LDH, C-MnCo, and C-MnCoCr PXRD patterns, respectively. The results confirmed that interlayer regions of H_2O, OH^-, and CO_3^{2-} have completely collapsed and are being decomposed during the calcination process. The process of dehydration, dehydroxylation, and decarboxylation occurred during the calcination process, which affected the interlayer spacing, hence collapsing and turning to mixed oxides. These can be proven where the LDH peaks at (003), (110), (113), and (116) were diminished.

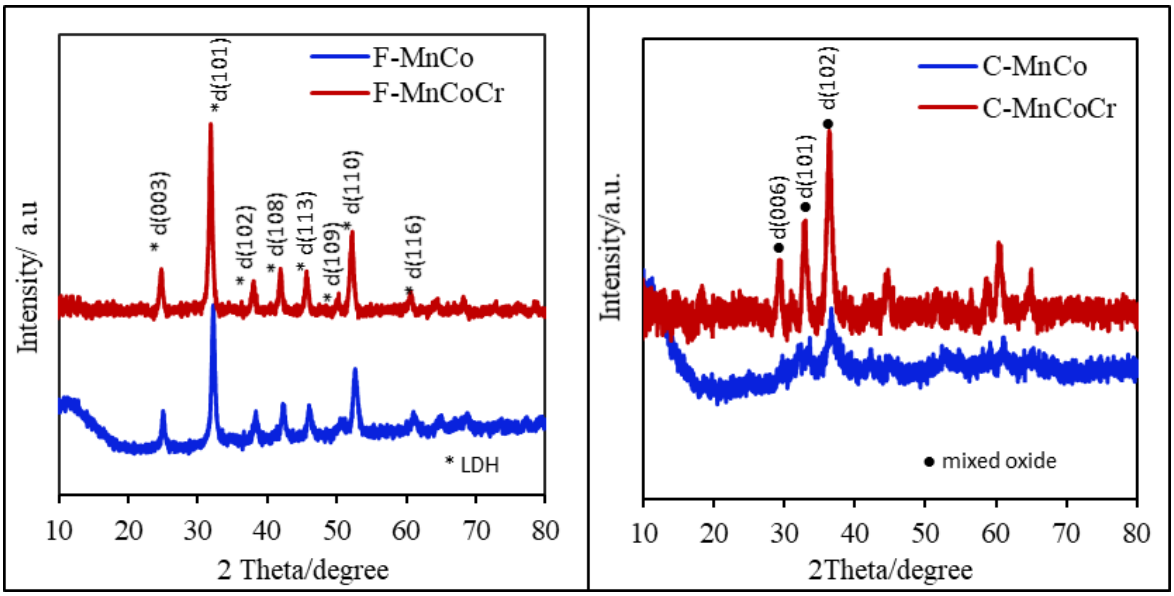

Figure 1. PXRD diffraction for fresh (a) and calcined (b) LDH with formation of mixed oxides.

The production of mixed oxide during calcination is shown by obvious diffraction at 37° for C-MnCo and 29°, 32°, and 36° for C-MnCoCr in **Figure 1(b)**. The diffraction peaks observed are consistent with the standard pattern for mixed metal oxides, as indexed by JCPDS card no. 45-0946 [18]. The C-MnCoCr PXRD patterns feature sharper peaks than C-MnCo, indicating that C-MnCoCr has higher crystallinity than C-MnCo. The textural features d spacing and the LDH lattice parameter are shown in **Table 1.**

With the addition of a tertiary component in ternary LDHs, there could be further changes in interlayer spacing. In LDH's structure, positively charged layers are separated by anionic species, forming a structure with distinct interlayer spaces. The introduction of a third element (Cr) has proven remarkably influential effect on the arrangement of these layers, hence potentially leading to modifications in the distance between them. These can be confirmed as the fresh ternary F-MnCoCr sample produced a slightly higher d-spacing between crystal lattice planes in a crystalline material compared to the binary F-MnCo sample. This analysis provides valuable information about the arrangement of atoms or molecules within the crystal lattice. Changes in d-spacing can indicate variations in the crystal structure, lattice parameters, or the presence of impurities. It is crucial to note that the specific effects of calcination on d-spacing will vary depending on the composition of the

DOI: https://doi.org/10.17509/ijost.v11i1.87940
p- ISSN 2528-1410 e- ISSN 2527-8045

ternary LDH, the calcination conditions (temperature, time, atmosphere), and the overall crystallographic alterations induced by the process [19]. In the context of ternary LDHs, changes in the lattice parameters might indicate structural differences, such as the introduction of various metal cations (MnCoCr), and this drastically alters the layer stacking sequence and, as a result, the interlayer spacing increases [18]. The fresh ternary LDH comprises water molecules and anions that contribute to the expansion of the original lattice structure. During calcination, these interlayer species are often removed by dehydroxylation and decarbonation processes. As these species (water and anions) are eliminated, the layers compress, leaving more distance between them. This process may result in an expansion of the interlayer region and may manifest as a surge in lattice parameters, as shown in **Table 1.**

Table 1. The textural properties of the d spacing and lattice parameter of binary and ternary LDH.

Systems	Materials	d spacing (λ)	Lattice Parameter (A°)	
			a	c
Binary	F-MnCo LDH	3.5	8.3	10.5
	C-MnCo LDH	2.4	2.7	3.5
Ternary	F-MnCoCr LDH	3.6	2.7	4.4
	C-MnCoCr LDH	17.1	8.3	10.5

The TGA investigations confirmed that the temperatures employed for calcination samples should be set at 375 and 425 °C, respectively. **Table 2** presents a summary of the thermogravimetric data for binary and ternary LDH. Three weight losses were observed in both binary and ternary samples the temperature range of 98-425 °C. Dehydration happened at 98-125 °C, releasing the physically absorbed water and exposing the metal catalysts to high temperatures. This finding is consistent with the results of the study mentioned in another reference [1]. The second weight loss occurred between 225-280 °C and was ascribed to the dehydroxylation process caused by the disintegration of LDH, which resulted in the elimination of interlamellar water molecules and ions [20]. The final major weight loss for F-MnCo occurred at 375 °C, which is linked to the disintegration of the Mn-Co LDH molecule, also known as decarbonation or decarboxylation [21]. The ternary F-MnCoCr decomposed at 425 °C, indicating the decomposition temperature of the Mn-Co-Cr LDH. The results closely paralleled those in references (Zhang et al., 2019) and [15].

The addition of binary and ternary metals to LDH structures has a substantial effect on their decomposition temperatures. The addition of binary metal cations has proven to modify the bonds between metal and oxygen, hence impacting the thermal stability [11]. Ternary LDHs, which include a third metal or have a changed anionic composition, exhibit intricate decomposition characteristics. The presence of ternary cations has created stronger bonding and coordination effects between the layers, requiring higher temperatures for decomposition to occur [22].

Therefore, the progressive increase in decomposition temperature from binary to ternary LDHs demonstrates that the addition of Cr not only modifies the thermal stability profile but also improves the structural resilience of the material. These findings align with earlier studies [22, 15] and affirm that multi-metal LDHs can be strategically tailored to optimize their thermal and physicochemical properties for applications such as catalysis, adsorption, and energy storage. The results also validate the calcination temperatures chosen (375 °C for MnCo and 425 °C for MnCoCr), ensuring complete structural transformation into mixed metal oxides without premature collapse or loss of functional integrity.

DOI: https://doi.org/10.17509/ijost.v11i1.87940
p- ISSN 2528-1410 e- ISSN 2527-8045

Table 2. The thermogravimetric analysis data of binary and ternary LDHs measured by TGA.

Systems	Materials	Decomposition (°C)	Weight loss stages	First weight loss (°C) (dehydration)	Second weight loss (°C) (dehydroxylation)	Third weight loss (°C)
Binary	F-MnCo LDH	375	Three	98	280	375
Ternary	F-MnCoCr LDH	425	Three	125	225	425

A pore distribution investigation was conducted using a QuantaChrome Autosorb device in the presence of nitrogen gas at a temperature of 77 Kelvin. **Figures 2(a) and (b)** show a type IV isotherm accompanied by an H3 hysteresis loop. The surface area of F-MnCo and F-MnCoCr in **Table 3** exhibits a significant disparity in magnitude, with F-MnCoCr demonstrating a superior value of 112 m2/g. The result associated with the PXRD graph of F-MnCoCr demonstrates superior crystallinity in comparison to F-MnCo. Introducing Cr into the MnCo matrix, such as in MnCoCr, has further impacted the surface area and the pore size. Cr may alter the crystal structure and affect interlayer distances, leading to changes in both parameters. Cr doping can also influence the formation of specific phases with distinct porosity characteristics. The addition of Cr has enhanced the surface area and altered the surface properties of F-MnCoCr (ternary LDH) compared to F-MnCo (binary LDH). The interaction between the tertiary and binary layers, as well as their impact on the primary layers, can collectively contribute to adjustments in pore size. The findings indicate that the ternary LDH (F-MnCoCr) exhibited superior parameter values for surface area compared to the binary LDH (F-MnCo).

Following calcination, the surface area of C-MnCo remains mostly unaffected, yet C-MnCoCr experiences disturbance, resulting in a decrease in value (**Table 3**). The LDHs exhibited a mean surface area similar to the values reported in references (Tajuddin et al., 2022) and [16]. Although the surface area of both calcined LDHs remains unaffected and decreased, respectively, the pore size of the C-MnCo and C-MnCoCr has steadily increased from their fresh samples, respectively. The decrease in MnCoCr surface area after calcination may be ascribed to a variety of structural and chemical changes that occur throughout the process. Calcination, the process of heating a material to high temperatures (425 °C), has resulted in an array of physical and chemical changes [23]. Calcination causes crystallization, which leads to particle expansion and aggregation in the interlayer [24], consequently reducing the total surface area of individual particles. Sintering is a high-temperature process that occurs during the calcination process [25]. As a consequence, the overall surface area may decrease. Aside from that, the calcination of MnCoCr may result in phase shifts, possibly resulting in a more compact or less porous structure.

It can additionally result in the removal of volatile components, leading to a decrease in porosity and surface area [26]. At high temperatures, calcination may cause chemical processes that culminate in the production of more stable compounds or phases, such as mixed oxides. These processes involve atom rearrangement and may result in a decrease in accessible surface area [25].

DOI: https://doi.org/10.17509/ijost.v11i1.87940
p- ISSN 2528-1410 e- ISSN 2527-8045

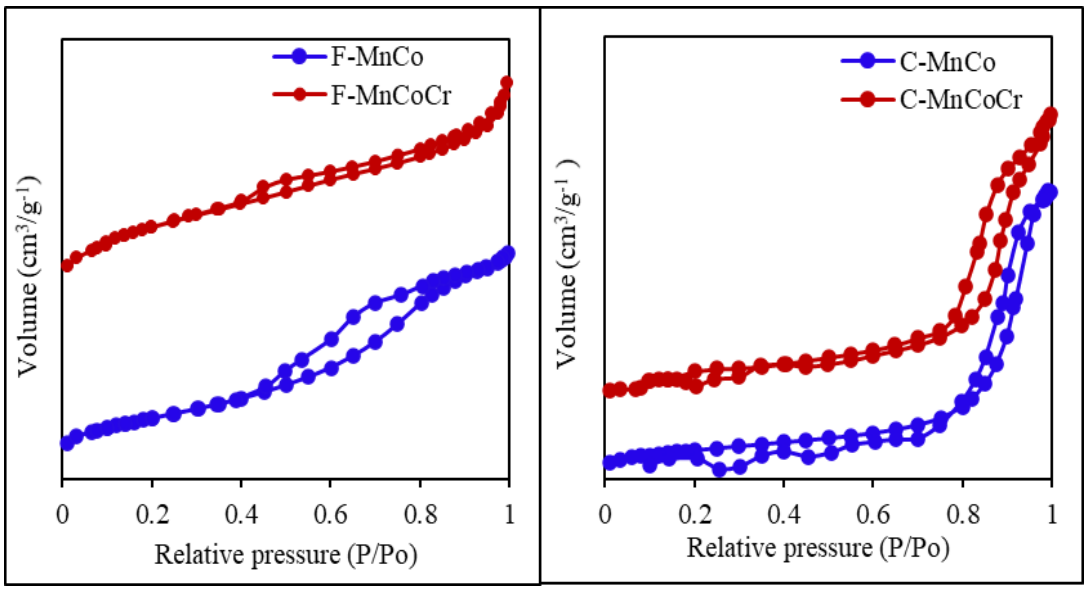

Figure 2. Nitrogen adsorption/desorption of isotherm linear plot of fresh (a) and calcined (b) LDHs consist of binary and ternary compounds.

Table 3. The summary of surface area, BJH pore size, and FESEM particle size of fresh and calcined binary and ternary LDH.

Systems	Materials	Surface area (m^2/g)	BJH Pore size (nm)		FESEM Mean particle size (nm)
			Absorption	Desorption	
Binary	F-MnCo LDH	71	6	5	115
	C-MnCo LDH	72	18	13	15
Ternary	F-MnCoCr LDH	112	5	5	289
	C-MnCoCr LDH	53	12	13	30

Figures 3(a) and (**b)** depict the morphology of both fresh and calcined binary and ternary LDHs observed by FESEM. The binary LDH (F-MnCo) exhibits agglomeration, resulting in an irregular shape, as presented in **Figure 3(a)**. In contrast, the structure of ternary LDH (fresh and calcined) shows a more uniform distribution and less interconnection with higher particle size; 289 nm and 30 nm for both fresh and calcined ternary LDH, respectively (**Figure 3(b)** and **Table 3**). The previous studies [26] reported the presence of an uneven edge in the LDH structure, but our study only observed a clumped and irregular structure. Despite the apparent clustering of F-MnCo and F-MnCoCr, the pore size progressively increases during the calcination of LDHs, as shown in **Table 3**. Therefore, this clarifies that while the pore diameters are larger than those of fresh, they do not result in any pore blockage. In addition to the ternary LDH synthesis process, the degree of crystallinity also significantly influences the morphology of LDH as the results are correlated in PXRD dan FESEM data.

Figure 4 presents field emission scanning electron microscopy (FESEM) images of the ternary MnCoCr layered double hydroxide (LDH) samples in their fresh (F-MnCoCr, image a) and calcined (C-MnCoCr, image b) states, both captured at 4000× magnification. The morphological differences between these two samples are distinct and highlight the structural evolution induced by the calcination process.

DOI: https://doi.org/10.17509/ijost.v11i1.87940
p- ISSN 2528-1410 e- ISSN 2527-8045

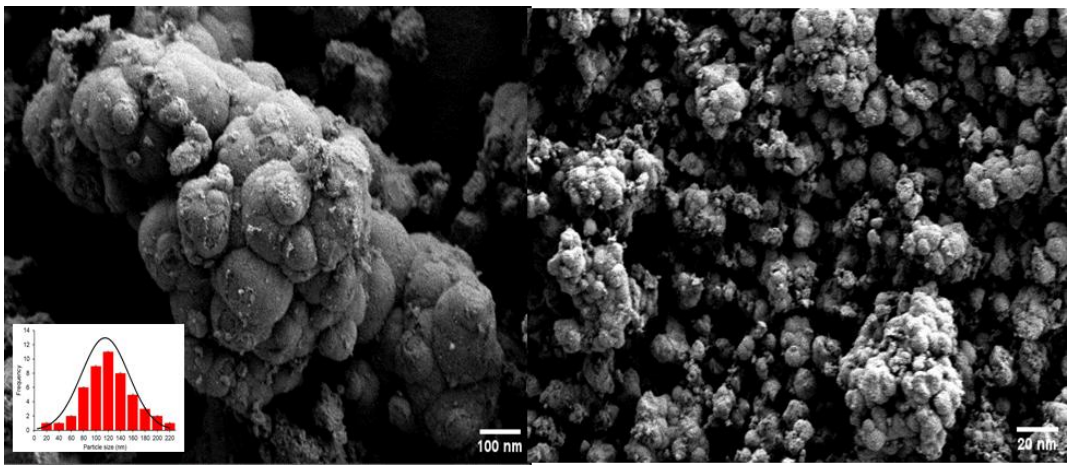

Figure 3. FESEM images for samples binary F-MnCo (a) and C-MnCo (b) at 4k magnification.

In **Figure 4(a)**, the F-MnCoCr sample exhibits a highly aggregated morphology with irregularly shaped, bulky clusters. The particles appear loosely packed, with significant surface roughness and non-uniform distribution. This suggests incomplete crystallization and uncontrolled particle growth, likely due to heterogeneous nucleation sites during the alkali-free synthesis. The inset histogram confirms this observation, showing a broad particle size distribution centered around 300 nm, with some particles exceeding 600 nm. This indicates a lack of uniformity and possible agglomeration, common in freshly precipitated LDH systems.

By contrast, **Figure 4(b)** shows the microstructure of C-MnCoCr after thermal treatment. The morphology transitions to more uniform, spherical particles with smoother surfaces and more compact packing. The calcination process appears to enhance structural reorganization and densification, possibly due to the removal of interlayer water and decomposition of carbonate anions, leading to the formation of mixed metal oxides. The corresponding particle size distribution shows a much narrower range, centered around 30–40 nm, indicating a significant reduction in particle size and improved homogeneity.

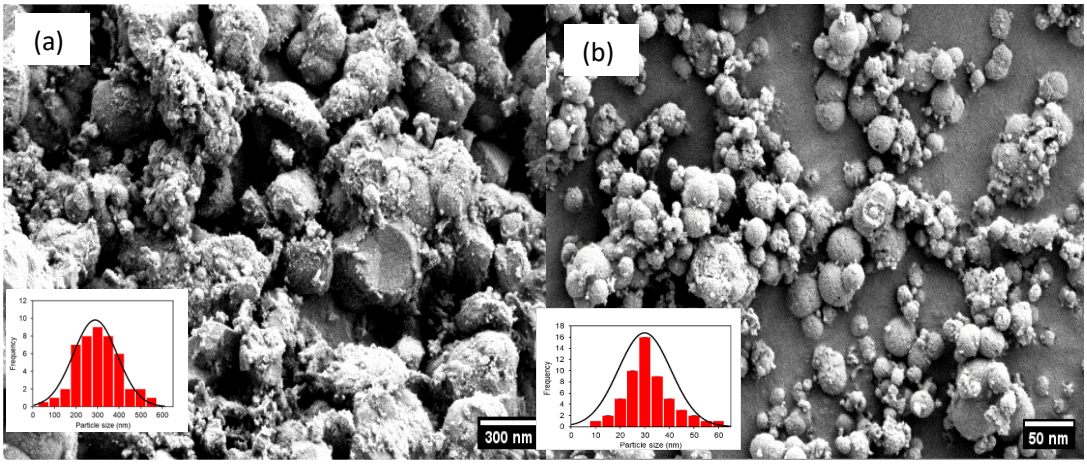

Figure 4. FESEM images for samples ternary F-MnCoCr (a) and C-MnCoCr (b) at 4k magnification.

This morphological refinement from fresh to calcined state not only demonstrates the effectiveness of calcination in tuning particle structure but also reinforces the impact of Cr in facilitating a more ordered transition. The size reduction and improved uniformity in C-

DOI: https://doi.org/10.17509/ijost.v11i1.87940
p- ISSN 2528-1410 e- ISSN 2527-8045

MnCoCr may contribute to enhanced surface area and reactivity traits highly desirable in catalytic applications.

The disparities in the morphology between MnCo and MnCoCr may be attributed to the addition of chromium (Cr) as a third metal cation in MnCoCr introduces a different element with its size, electronic properties, and crystal structure. The addition of Cr modifies the interactions between metal cations, as well as the nucleation, development, and organization of crystal structures, resulting in increased particle size, as shown in **Figure 5.** Cr, which has a bigger atom than Mn or Co, alters the interlayer gap in the LDH structure, causing it to expand or shrink depending on how it interacts with surrounding hydroxide layers. The introduction of foreign species (such as Cr in the preceding context) during crystal formation alters lattice characteristics, resulting in changes in d-spacing, as previously observed and described [27, 28]. Cr has induced lattice expansion, as shown by the increase in d-spacing (**Table 1**), morphology (**Figures 3(a)-(b)** and **4(a)-(b)**), and particle size. Changes in lattice properties and interatomic distances may occur during crystal growth, notably in the nucleation and following phases [29]. Cr functions as a crystal formation catalyst, allowing LDH crystals to form and grow more easily. Its distinct electronic structure may improve the LDH's capacity to interact with anions or ligands during synthesis, especially in ion-exchange procedures [10]. Cr may also change the surface charge of LDH particles, influencing their reactivity with surrounding anions or ligands, thereby improving their functioning in a variety of applications.

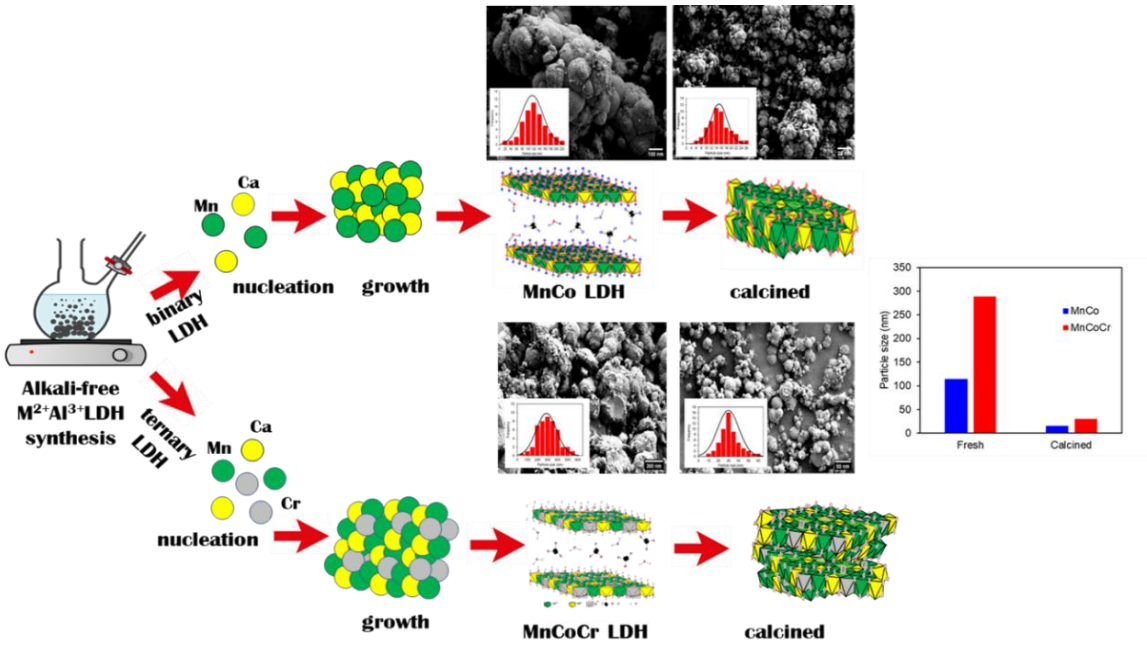

Figure 5. Schematic illustration of a proposed evolution process of binary and ternary LDH hierarchical architecture leading to the enhancement of the aggregated network along with the increment of the particle growth.

The presence of Cr not only influences the cationic framework but also has a profound effect on the interlayer region of the LDH, where it can modify the spacing between hydroxide layers by altering electrostatic forces and hydrogen bonding interactions with intercalated anions and water molecules. As a result, the interlayer gap may either expand or contract, depending on the spatial and electronic interactions induced by Cr's presence. Furthermore, the incorporation of a foreign cation such as Cr introduces localized lattice distortions and modifies the symmetry of the crystal lattice, leading to observable changes in basal spacing (d-spacing). These structural variations are not merely of academic interest—they directly

DOI: https://doi.org/10.17509/ijost.v11i1.87940
p- ISSN 2528-1410 e- ISSN 2527-8045

impact the material's surface properties, accessibility of active sites, and suitability for catalytic applications. Thus, the integration of Cr into the LDH structure plays a multifaceted role, acting both as a structural modulator and a functional enhancer within the ternary MnCoCr LDH system.

The FTIR analysis of MnCo and MnCoCr LDHs was performed on both fresh and calcined samples and tabulated in **Table 4**. The weak broad absorption peaks at 3323.60, 3350.20, 3356.16, and 3350.00 cm^{-1} correspond to the OH group in the interlayer of carbonate ions and water molecules [29, 30]. In contrast to the calcined samples, both fresh binary and ternary samples produced a dense O-H wide signal. This is due to the presence of OH^-/H_2O molecules in new samples, which are found between interlamellar layers. These compounds were exposed to interlayer removal and decomposition during calcination, resulting in layers that collapsed and formed mixed oxide, as shown by PXRD data. The FTIR spectra of both calcined binary and ternary materials are less dense than fresh samples, indicating a successful calcination procedure [30].

The tiny remaining peak of O-H might be due to trapped ambient air on the samples, which can be removed by heating before analysis. Weak peaks at 1754.30, 1758.50, 1803.23, and 1632.00 cm^{-1} indicate C=O stretching for both binary Mnco and ternary MnCoCr, with a lower absorption peak at 1500 cm^{-1} corresponding to O-C-O bending. Most absorption peaks in all samples were relatively comparable, with a slightly distinct LDH band at 950 to 720 cm^{-1}. The absorption bands below 1000 cm^{-1} correspond to metal oxide stretching modes in the brucite-like layer or may be simplified as LDH bands [16]. A similar distortion of LDH wavelength was discovered in [1, 13] at 816-854 and 784-683 cm^{-1}.

Table 4. The summary of characteristic bands and wavenumbers of binary and ternary LDHs obtained from this study and previous references.

Systems	Materials	Characteristic band	Wavenumber (cm^{-1}) (this study)	Wavenumber (cm^{-1}) (ref)	References
Binary	F-MnCo LDH	O-H stretching	3323.60	3445.37	[30]
		C=O stretching	1754.30	1500	[16]
		CO_3 bending	1371.10	1363-1384	[31]
		Mn-O / Co-O stretching	861.0	854.41	
		Mn-Co LDH bending	722.50	784-683	
	C-MnCo	O-H stretching	3356.16	3448	[30]
		C=O stretching	1803.27	1500	[32]
		CO_3 bending	1390.60	1363-1384	[31]
		Mn-O / Co-O bending	861.00	854.41	[33]
		Mn-Co LDH bending	726.15	784-683	
Ternary	F-MnCoCr LDH	O-H stretching	3335.20	3448	[30]
		C=O stretching	1758.50	1500	[8]
		CO_3 bending	1370.20	1363-1384	[32]
		Mn-O / Co-O stretching	839.90	854.41	[25]
		Mn-Co-Cr LDH bending	722.50	784-683	

DOI: https://doi.org/10.17509/ijost.v11i1.87940
p- ISSN 2528-1410 e- ISSN 2527-8045

Table 4 (Continue). The summary of characteristic bands and wavenumbers of binary and ternary LDHs obtained from this study and previous references.

Systems	Materials	Characteristic band	Wavenumber (cm^{-1}) (this study)	Wavenumber (cm^{-1}) (ref)	References
	C-MnCoCr	O-H stretching	3350.00	3448	[30]
		C=O stretching	1632.00	1500	[32]
		CO_3 bending	1405.00	1363-1384	
		Mn-Co-Cr LDH bending	943.10	816-854	

4. CONCLUSION

This study emphasizes the critical role of chromium in enhancing the structural and functional properties of layered double hydroxides (LDHs). The ternary MnCoCr LDHs exhibited superior crystallinity, larger particle size, and more uniform morphology compared to binary MnCo LDHs. Chromium incorporation significantly influenced interlayer spacing, crystal growth, and thermal stability, as supported by PXRD and FESEM analyses. These modifications are essential for improving material performance in catalysis and other applications. Importantly, this work demonstrates how careful control of metal composition in LDHs enables the precision engineering of structure–property relationships, offering a strategic pathway for developing high-performance, application-specific materials.

5. ACKNOWLEDGMENT

This research was funded by the MYPAIR-STFC: ISIS MUON NEUTRON SOURCE, UK Grant under number 100-TNCPI/INT 16/6/2 (041/2024), awarded by Science and Technology Facilities Council (STFC), United Kingdom, and the Ministry of Higher Education (MOHE), Malaysia. The authors gratefully acknowledge the support from the Faculty of Applied Sciences, Universiti Teknologi MARA (UiTM) for providing great facilities and assistance throughout the research.

6. AUTHORS' NOTE

The authors declare that there is no conflict of interest regarding the publication of this article. The authors confirmed that the paper was free of plagiarism.

7. REFERENCES

[1] Zhang, W., Liang, Y., Wang, J., Zhang, Y., Gao, Z., Yang, Y., and Yang, K. (2019). Ultrasound-assisted adsorption of congo red from aqueous solution using $MgAlCO_3$ layered double hydroxide. *Applied Clay Science*, *174*, 100–109.

[2] Cavani, F., Trifirò, F., and Vaccari, A. (1991). Hydrotalcite-type anionic clays: Preparation, properties and applications. *Catalysis Today*, *11*(2), 173–301.

[3] Tajuddin, N. A., Sokeri, E. F., Kamal, N. A., and Dib, M. (2023). Fluoride removal in drinking water using layered double hydroxide materials: Preparation, characterization and the

current perspective on IR4.0 Technologies. *Journal of Environmental Chemical Engineering*, *11*(3), 110305.

[4] Razzaq, A., Ali, S., Asif, M., and In, S.-I. (2020). Layered double hydroxide (LDH) based photocatalysts: An outstanding strategy for efficient photocatalytic CO_2 Conversion. *Catalysts, 10*(10), 1185.

[5] Lee, C., Madhusudan, P., and Kim, J.-O. (2024). Recovery of phosphate using a zinc oxide/hydroxide and lanthanum hydroxide nanoflower adsorbent prepared via co-precipitation in water. *Separation and Purification Technology*, *330*, 125313.

[6] Mohamed, E. A., Betiha, M. A., and Negm, N. A. (2023). Insight into the recent advances in sustainable biodiesel production by catalytic conversion of vegetable oils: Current trends, challenges, and prospects. *Energy and Amp; Fuels, 37*(4), 2631–2647.

[7] Hidalgo, P., Toro, C., Ciudad, G., and Navia, R. (2013). Advances in direct transesterification of microalgal biomass for biodiesel production. *Reviews in Environmental Science and Bio/Technology, 12*(2), 179–199.

[8] Tajuddin, Nazrizawati A., Manayil, J. C., Lee, A. F., and Wilson, K. (2022). Alkali-free hydrothermally reconstructed nial layered double hydroxides for catalytic transesterification. *Catalysts, 12*(3), 286.

[9] Huang, Y., Liu, C., Rad, S., He, H., and Qin, L. (2022). A comprehensive review of layered double hydroxide-based carbon composites as an environmental multifunctional material for wastewater treatment. *Processes, 10*(4), 617-633.

[10] Li, X., Yang, J., Chen, J., Sun, J., Liu, J., Cui, X., and Zou, L. (2024). High-performance ternary nifeco-LDH nanosheets for supercapacitors by cation modulation and sodium dodecyl sulfonate intercalation. *Journal of Materials Chemistry A, 12*(5), 2887–2901.

[11] Huiyuan, T., Yang, L., Mengyan, X., Baoyu, C., Chang, L., Xiuhong, D., Zehua, W., Xianying, D., and Jiehu, C. (2024). The enhanced adsorption of layered double hydroxides modification from single to ternary metal for fluoride by tea-assisted hydrothermal method. *Arabian Journal of Chemistry, 17*(3), 105645.

[12] Nasir, M. H., Niaz, H., Yunus, N., Ali, U., Khan, S., Butt, T. M., Naeem, H., Li, H., Habila, M. A., and Janjua, N. K. (2024). Calcium-, magnesium-, and yttrium-doped lithium nickel phosphate nanomaterials as high-performance catalysts for electrochemical water oxidation reaction. *Nanotechnology Reviews, 13*(1), 20230166.

[13] Tajuddin, N. A., Saleh, R., Manayil, J. C., Isaacs, M., Parlett, C. M. A., Lee, A. F., and Wilson, K. (2019). Hydrothermal reconstructing routes of alkali-free ZnAl layered double hydroxide: A characterisation study. *Solid State Phenomena*, 290, 168–176.

[14] Mohd Agus, R. A., Deraman, S. K., and A. Tajuddin, N. (2021). Synthesis and characterization of two-dimensional (2D) nanosheet zinc aluminum layered double hydroxide (Zn/Al LDH) via an alkali-free route. *Science Letters*, *15*(1), 91-98.

[15] Kandula, S., Shrestha, K. R., Kim, N. H., and Lee, J. H. (2018). Fabrication of a 3D hierarchical sandwich co9s8/α-mns@n–c@mos2 nanowire architectures as advanced electrode material for high performance hybrid supercapacitors. *Small, 14*(23), 1800291.

DOI: https://doi.org/10.17509/ijost.v11i1.87940
p- ISSN 2528-1410 e- ISSN 2527-8045

[16] Ibrahim, E. H., Tajuddin, N. A., & Hamzah, N. (2019). Synthesis and characterization of alkali free Mg-Al layered double hydroxide for transesterification of waste cooking oil to biodiesel: Effect of Mg-Al ratio. *International Journal Engineering Technology*, *7*, 154-157.

[17] Tong, D. S., Liu, M., Li, L., Lin, C. X., Yu, W. H., Xu, Z. P., and Zhou, C. H. (2012). Transformation of alunite residuals into layered double hydroxides and oxides for adsorption of acid red G Dye. *Applied Clay Science, 70*, 1–7.

[18] Sun, H., Heo, Y.-J., Park, J.-H., Rhee, K. Y., and Park, S.-J. (2020). Advances in layered double hydroxide-based ternary nanocomposites for photocatalysis of contaminants in water. *Nanotechnology Reviews, 9*(1), 1381–1396.

[19] Tang, Z., Qiu, Z., Lu, S., and Shi, X. (2020). Functionalized layered double hydroxide applied to heavy metal ions absorption: A Review. *Nanotechnology Reviews, 9*(1), 800–819.

[20] Saegher, T. D., Lauwaert, J., Hanssen, J., Bruneel, E., Van Zele, M., Van Geem, K., De Buysser, K., and Verberckmoes, A. (2020). Monometallic cerium layered double hydroxide supported Pd-Ni nanoparticles as high performance catalysts for lignin hydrogenolysis. *Materials, 13*(3), 691-714.

[21] Chagas, L. H., De Carvalho, G. S. G., Do Carmo, W. R., San Gil, R. A. S., Chiaro, S. S. X., Leitão, A. A., Diniz, R., De Sena, L. A., and Achete, C. A. (2015). MgCoAl and NiCoAl LDHS synthesized by the hydrothermal urea hydrolysis method: Structural characterization and thermal decomposition. *Materials Research Bulletin*, 64, 207–215.

[22] Tiwari, A., Novak, T., Bu, X., Ho, J., and Jeon, S. (2018). Layered ternary and quaternary transition metal chalcogenide based catalysts for water splitting. *Catalysts, 8*(11), 551-580.

[23] Benito, P., Labajos, F. M., and Rives, V. (2009). Microwaves and layered double hydroxides: A smooth understanding. *Pure and Applied Chemistry*, 81(8), 1459–1471.

[24] Zhao, Y., Xu, L., Guo, M., Li, Z., Xu, Z., Ye, J., Li, W., and Wei, S. (2022). Effects of calcination temperature on grain growth and phase transformation of nano-zirconia with different crystal forms prepared by hydrothermal method. *Journal of Materials Research and Technology*, *19*, 4003–4017.

[25] Yuan, J. P., Chen, N., Hu, C. C., Liu, B., and Song, K. X. (2024). Enhanced microwave dielectric properties in one-step cold sintered LiF ceramics via pre-calcination treatment. *Ceramics International*, *50*(23), 51625-51630.

[26] Hosseini, S. S., Mehrpooya, M., and Jahangir, M. H. (2024). Advancing alkaline fuel-cells cathode through synergistic catalyst design: Integrated LDH-derived ternary mixed metal oxide with n/CO multi-doped reduced graphene oxide. *Materials Chemistry and Physics*, 314, 128838.

[27] Falsaperna, M., Arrigo, R., Marken, F., and Freakley, S. J. (2024). Alkali containing layered metal oxides as catalysts for the oxygen evolution reaction. *ChemElectroChem, 11*(8), .

[28] Do, V.-H., and Lee, J.-M. (2024). Surface Engineering for stable electrocatalysis. *Chemical Society Reviews, 53*(5), 2693–2737.

DOI: https://doi.org/10.17509/ijost.v11i1.87940
p- ISSN 2528-1410 e- ISSN 2527-8045

[29] Hong, C., Liu, Z., Chen, T., and Wu, A. (2023). Two-dimensional layered nanomaterials for tumor diagnosis and treatment. *Medical Review, 3*(3), 205–208.

[30] Zeng, X., and Yang, Z. (2020). Synthesis of CaZnAl-CO3 ternary layered double hydroxides and its application on thermal stability of Poly (vinyl chloride) resin. *Journal of Central South University, 27*(3), 797–810.

[31] Xuan, H., Guan, Y., Han, X., Liang, X., Xie, Z., Han, P., and Wu, Y. (2020). Hierarchical MnCo-LDH/rgo@nico2s4 heterostructures on Ni foam with enhanced electrochemical properties for battery-supercapacitors. *Electrochimica Acta*, 335, 135691.

[32] Tajuddin, N., Manayil, J., Isaacs, M., Parlett, C., Lee, A., and Wilson, K. (2018). Alkali-free Zn–Al layered double hydroxide catalysts for triglyceride transesterification. *Catalysts, 8*(12), 667-678.

[33] Wu, S., Zhang, J., Sun, C., and Chen, J. (2020). Synthesis of MNO2/NiCo-layered double hydroxide hybrid as electrode materials for Supercapacitor. *Journal of Inorganic and Organometallic Polymers and Materials, 30*(8), 3179–3187.

DOI: https://doi.org/10.17509/ijost.v11i1.87940
p- ISSN 2528-1410 e- ISSN 2527-8045